Sub-10-nm Pd Nanosheets with Renal Clearance for Efficient Near-Infrared Photothermal Cancer Therapy

*Shaoheng Tang, Mei Chen, and Nanfeng Zheng**

***E**fficient renal clearance is of fundamentally important property of nanoparticles for their in vivo biomedical applications. In this work, we report the successful synthesis of ultra-small Pd nanosheets (SPNS) with an average diameter of 4.4 nm and their application in photothermal cancer therapy using a near infrared laser. The ultra-small Pd nanosheets have strong optical absorption in the NIR region and high photothermal conversion efficiency (52.0%) at 808 nm. After being surface-functionalized with reduced glutathione (GSH), the SPNS-GSH was administered to mice to investigate the biodistribution, photothermal efficacy and tumor ablation in vivo. The in vivo photothermal therapy studies clearly demonstrate that surface modification with GSH allows the nanosheets to exhibit prolonged blood circulation and thus high accumulation in tumors. Upon 808 nm NIR irradiation, the tumors can be completely ablated. More importantly, with the size below the renal filtration limit (<10 nm), the GSHylated Pd nanosheets can be nicely cleared from body through the renal excretion route and into urine. Together with the high efficacy of NIR photothermal therapy, the unique renal clearance properties make the ultra-small Pd nanosheets promising for practical use in photothermal cancer therapy.*

1. Introduction

During the past decade, nanomaterials with photothermal effect in near-infrared (NIR) region have attracted considerable attention for their promising applications in photothermal cancer therapy.[1–3] Such kind of nanomaterials are capable of absorbing NIR light and then efficiently converting the absorbed light into heat.[4] NIR light is highly desirable for in vivo imaging and therapeutic applications owing to the minimal optical absorption of blood and soft tissue in this region to allow the maximal tissue penetration.[5] When photothermal transducers accumulate in the tumor, they absorb NIR light and produce localized cytotoxic heat to ablate tumor. Obviously, biocompatible and efficient NIR photothermal nanomaterials are the key component of NIR photothermal cancer therapy. Up to date, significant progress has been made in the synthesis of photothermal agents,[6–15] such as Au nanoshells,[16] Au nanorods,[17] Au nanocages,[18] graphene nanosheets,[19] carbon nanotubes,[20] and Pd nanosheets.[21]

Although several plasmonic nanomaterials are subjected to investigation, and even Au nanoshells and nanorods have been explosively employed for clinical trials.[22–24] the preparation of nanomaterials that possess high photothermal efficiency and efficient renal clearance is still a great challenge. It is well known that the diameter of nanoparticles with efficient renal clearance is required to be smaller than 10 nm,[25] which is the renal filtration limit. However, up to now, limited by the preparation methods or structural requirement to have efficient photothermal effect in NIR, such as structural anisotropy or hollow structure for plasmonic metal nanomaterials,

S. H. Tang, M. Chen, Prof. N. F. Zheng
State Key Laboratory for Physical Chemistry of Solid Surfaces
Collaborative Innovation Center of Chemistry for Energy Materials
and Department of Chemistry
College of Chemistry and Chemical Engineering
Xiamen University
Xiamen 361005, China
Fax: (+86)592–218–3047
E-mail: nfzheng@xmu.edu.cn

DOI: 10.1002/smll.201303631

none of the reported NIR photothermal nanomaterials meet such a size requirement (e.g., gold nanorods with ≈50 nm in length,[26] gold nanoshells with more than 100 nm in diameter,[27] gold nanocages with ≈48 nm in edge length,[28] carbon nanotubes with 50–300 nm in lengths,[29] and graphene with 10–50 nm in diameter[14]. Therefore, it is crucial for clinical application that agents administered for diagnostic or therapeutic purposes could be completely cleared from the human body within a reasonable period. The development of nanomaterials with high photothermal efficiency and optimal clearance characteristics as well to minimize toxicity risks is highly desirable for photothermal cancer therapy.

In this study, we report the successful synthesis of ultra-small Pd nanosheets (SPNS) with an average diameter of ≈4.4 nm and their application in NIR photothermal cancer therapy. The SPNS not only have ultra-small size, which is thoroughly below the filtration-size threshold (10 nm), but also exhibit strong absorption and efficient photothermal conversion of NIR light. After surface-functionalized with reduced glutathione (GSH), the SPNS-GSH was administered to mice to investigate the biodistribution, photothermal efficacy and tumor ablation in vivo. To comprehensively evaluate the performances of SPNS-GSH as a photothermal therapy agent in vivo, we also investigated the clearance characteristics and security of the particles after photothermal treatments. With ultra-small size and strong absorption of light in NIR region, the SPNS exhibits great potential in application of photothermal therapy.

2. Results and Discussion

In a typical synthesis of small size Pd nanosheets, palladium(II) acetylacetonate, poly(vinylpyrrolidone) (PVP) and sodium bromide were dissolved in a mixed solvent consisting of water and organic solvents, such as dimethylacetamide (DMAC) and *N,N*-dimethylpropionamide (DMP). The resulting homogeneous solution was transferred to a glass pressure vessel. After being charged with CO to 1 bar, the vessel was heated from room temperature to 100 °C and kept at this temperature for 2 h with stirring. The resulting blue colloidal products were collected by centrifugation, and washed several times with ethanol and acetone. In our previous work, we reported the successful synthesis of plasmonic Pd nanosheets, with average size tunable from 42 to 320 nm and thickness of 1.8 nm, using *N,N*-dimethylformamide or benzyl alcohol as the solvent. The smallest nanosheets obtained in those systems were still too big to be cleaned out of body by renal. After administered into mice, the large sized Pd nanosheets were mainly trapped in reticuloendothelial system (RES; e.g. liver, spleen) and even made liver become dark blue. To be exerted through renal clearance, the size of Pd nanosheets should be less than 10 nm. Fortunately, by varying the reaction solvent and mixing ratio, we found that the mean particle size could be controlled below 21 nm (diagonal length) (**Figure 1**) while their thickness was still fixed at 1.8 nm. When DMP-water mixture was used as the solvent, reaction in the presence of both PVP and sodium bromide produced ultra-small Pd nanosheets with an

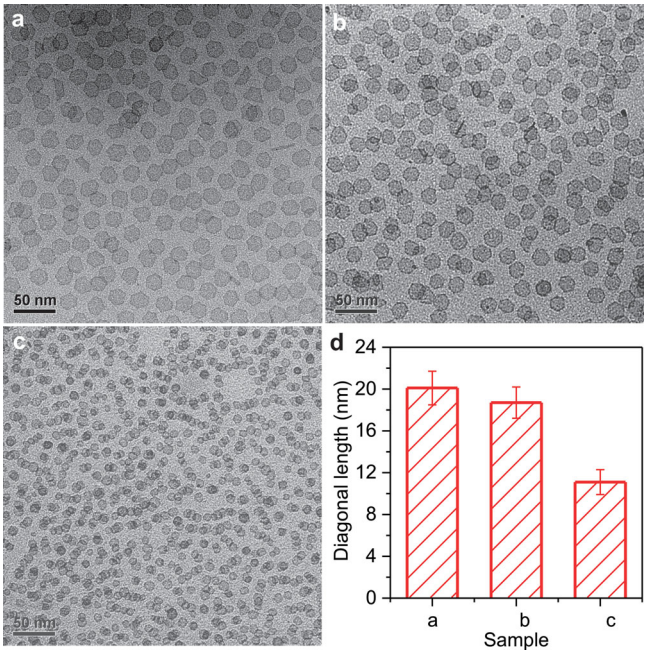

Figure 1. TEM images of the palladium nanosheets produced under different reaction conditions. (a) the Pd nanosheets with an average diagonal length of 20.1 nm, (b) the Pd nanosheets with an average diagonal length of 18.7 nm, (c) the Pd nanosheets with an average diagonal length of 11.1 nm, (d) Diagonal lengths of samples a–c.

average diameter of only ≈4.4 nm (**Figure 2**a) which is below the glomerular filtration-size threshold (10 nm) and thus particularly interesting for renal clearance studies. Noble metal nanostructures with such a small diameter are not expected

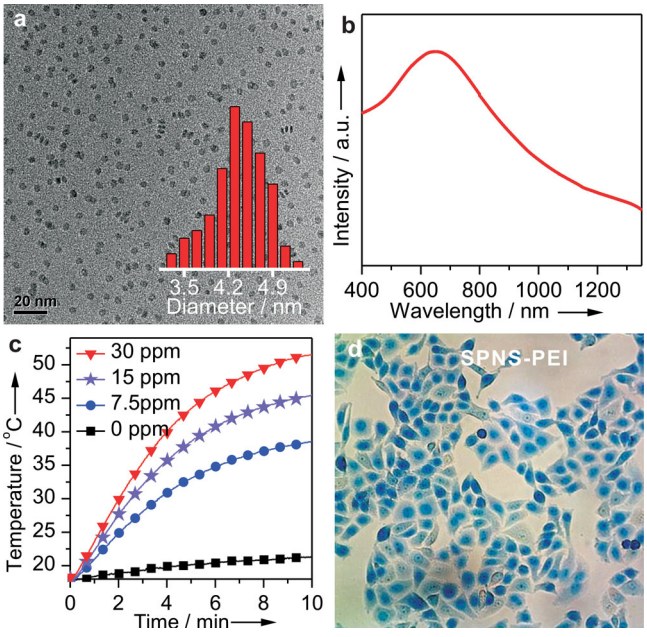

Figure 2. Characterization and NIR photothermal properties of SPNS. (a) TEM image of the SPNS. Inset: diameter distribution of the SPNS. (b) Absorption spectrum of the SPNS. (c) Photothermal effect of SPNS. The temperature versus time plots was recorded for various concentrations of SPNS upon irradiation by a 1-W laser. (d) Micrograph corresponding to photothermal therapy in vitro by SPNS-PEI at an optical power density of 0.8 W cm^{-2}. Dead cells are stained with trypan blue.

NANO MICRO small

to have strong SPR absorption in the NIR region. However, due to the two dimensional sheet structures, the 4.4-nm small Pd nanosheets displayed well-defined and strong SPR absorption with a peak around 700 nm. The intense absorption was nicely extended into the NIR region (Figure 2b).

To study the potential of using SPNS in photothermal therapy, the photothermal effect induced by NIR SPR absorption was investigated by monitoring the temperature changes of 1 mL aqueous solutions of various concentration of SPNS (0, 7.5, 15 and 30 ppm) irradiated by an 808 nm NIR laser (1 W). As shown in Figure 2c, in marked contrast to pure water, the temperature of the solution containing 30 ppm SPNS rose from 17.0 to 52.3 °C after 10 min of irradiation. According to Roper's method,[30] the 808 nm photothermal conversion efficiency of SPNS is as high as 52.0%, much higher than that of the large Pd nanosheets (LPNS) with edge length of 41 nm (27.6%) (see Supporting Information, Figure S1). This suggests that the SPNS should have an improved performance in photothermal therapy. After surface modified by polyethyleneimine (PEI) to increase the uptake by cells, the two kinds of Pd nanosheets (i.e., SPNS and LPNS) were applied to photothermal ablation of cancer cells. In our in vitro studies, liver cancer cells were incubated with various Pd nanosheets (20 μg mL^{-1}) for 12 h before the irradiation of an 808 nm laser at 0.8 W cm^{-2}. As illustrated in Figure 2d, 100% of the cells incubated with SPNS-PEI, were killed after 3 min irradiation. In comparison, the same irradiation killed only half of the cells incubated with the LPNS-PEI (see Supporting Information, Figure S2).

The high efficacy of SPNS in vitro photothermal therapy motivated us to further investigate the potential of the particles in tumor ablation in vivo using NIR laser. To date, while significant progress has been made toward the creation of the photothermal agents for anticancer therapy, applications of those nanomaterials are still severely hampered by their slow renal clearance and high, nonspecific accumulation in the RES after systematic administration.[31,32] It has been well-documented that many properties of nanomaterials, such as particle material, size, shape, surface chemistry and charge, influence the nonspecific accumulation and renal clearance. Among those properties, both the particle size and surface ligands play central roles.[33] According to Zheng's research, GSH (a tripeptide) can not only serve as capping agent to render the nanoparticles with relatively low affinities to serum proteins, leading to the desired stealthiness to the RES organs, but also contribute to efficient renal clearance of small-sized nanoparticles out of body.[33] We have therefore modified the SPNS with GSH for photothermal therapy.

Briefly, 0.5 mL DMF dispersion of SPNS (5 mg mL^{-1}) was added into 3 mL of 1.0 mg mL^{-1} GSH solution. The mixture was then shaken for 12 h at room temperature and we also further evaluated the dispersibility of nanoparticles in whole FBS by Small-angle X-ray scattering (SAXS). The pair distance distribution functions (PDDFs) were calculated from the fitting of curves using the model-free method of GIFT. The crossover of the decay of PDDF curve with the r-axis reflects the maximum dimension of the particle. The SPNS-GSH had smaller diameter (7.5 nm) than SPNS (11.0 nm) in whole serum (see Supporting Information, Figure S3), indicating that GSHylation can effectively prevent the particles from adsorption and opsonization by serum proteins.

To investigate the in vivo pharmacokinetics, male Sprague-Dawley (SD) rats were used. Because the characteristics of body clearance (CL) and renal clearance (CL_R) of drugs in SD rats were comparable to those in humans, SD rats have been hence widely chosen as the animal model in the study.[34,35] The SD rats weighing approximately 300 g were randomly divided into three groups (n = 3 per group). After a surgical operation, the cannulation of the jugular vein and carotid artery was performed for the pretreatment of rats.[34] The LPNS, SPNS and SPNS-GSH at a dose of 1 mg kg^{-1} were infused via the jugular vein to rats in three groups respectively. Blood sample (approximately 0.4 mL) was drawn via the carotid artery at different time points after administration. Each blood sample was lysed by aqua regia. After dilution, the Pd ion concentrations of the prepared solution were measured by inductively coupled plasma mass (ICP-MS) spectrometry. As clearly revealed in **Figure 3**a, the smaller size and modification by GSH were both helpful to prolong the circulation half-life of Pd nanosheets in blood. The circulation half-lives were remarkably increased from 0.08 h for LPNS to 1.25 h for SPNS-GSH.

It is well known that prolonged circulation facilitates the accumulation of nanomaterials in tumor via enhanced permeability and retention (EPR) effect. To further investigate their biodistributions, the three kinds of Pd nanosheets were injected into Balb/c mice bearing 4T1 tumors via tail vein. Mice were sacrificed at 24 hours post injection (p.i.), and their major organs (n = 3 per group) were weighed and lysed by aqua regia. The obtained homogenized tissue lysates were diluted and measured by ICP-MS to quantitatively determine the Pd concentrations. Compared to LPNS, the smaller SPNS showed low RES uptake, consistent with many previous studies that RES uptake of nanomaterials is very size-dependent and should be higher for larger sizes.[31] Obviously, after GSHylation, SPNS-GSH were successfully avoided to be rapidly cleared out of blood and trapped into the RES organs. As a result, a higher tumor accumulation was observed. Importantly, the total amount of Pd in SPNS-GSH formulation was significantly low in major

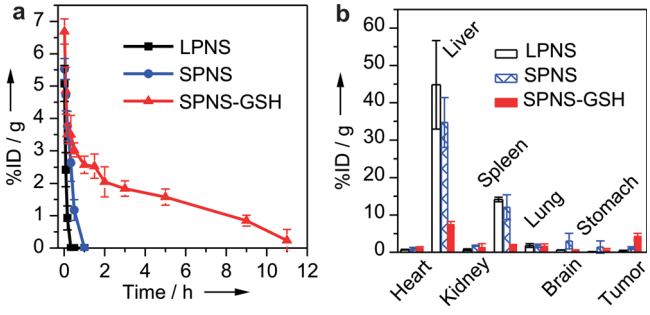

Figure 3. Size and functionalization-dependent blood circulation and biodistribution. (a) SPNS-GSH showed prolonged blood circulation compared with LPNS and SPNS. (b) Biodistribution of LPNS, SPNS and SPNS-GSH in various organs at 24 h p.i. Samples were measured using ICP-MS. Error bars were based on the standard error of the mean of triplicate samples.

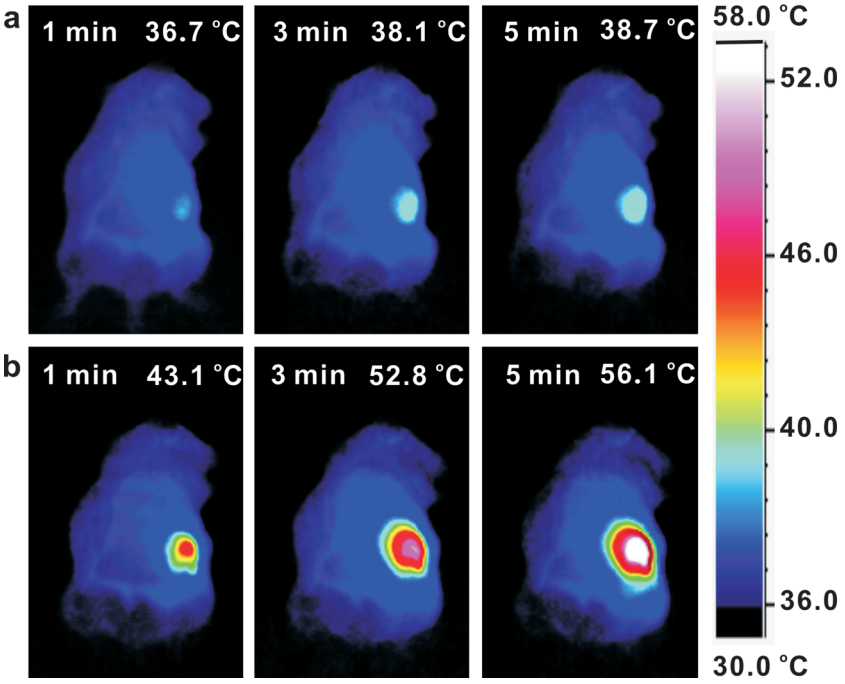

Figure 4. Photothermal effect *in vivo*. Thermographic images of saline-injected (a) and nanosheets-injected (b) Tumor-bearing mice at different time points. 200 μL of SPNS-GSH at a concentration of 2,000 ppm or saline was intravenously administrated to mice. At 24 h p.i., the tumor was exposed to an 808 nm laser at the density of 1 W cm^{-2}.

organs, indicating that plenty of the SPNS-GSH were rapidly excreted from body within the first 24 hours after administration (Figure 3b).

Motivated by the efficient passive targeting of SPNS-GSH in tumors, the in vivo photothermal effect was examined using the 4T1 tumor model on Balb/c mice. The mice bearing 4T1 tumors were randomly divided into two groups (n = 5 per group) that were intravenously injected with 200 μL of saline and SPNS-GSH in PBS (2 mg/mL), respectively. At 24-h p.i., the tumor was exposed to an 808 nm laser at the density of 1 W cm^{-2} for 5 min. During the irradiation, full-body thermographic images (**Figure 4**) and the temperature profile (see Supporting Information, Figure S4) were recorded by an infrared camera. For the nanosheets-injected mice, the tumor surface temperature increased rapidly to reach 56.1 °C within 5 min, in contrast to 38.7 °C for saline-injected mice.

To carry out *in vivo* photothermal therapy using Pd nanosheets, Balb/c mice were bilaterally injected in the hind flank with ≈2×10^6 4T1 cells. After the tumor volume had reached about 100 mm^3, the mice were randomly divided into four groups (n = 10 per group). Ten mice bearing 4T1 tumor were injected with 200 μL of SPNS-GSH at 2 mg mL^{-1}. Another 10 mice without SPNS-GSH injection were used as control. At 24 h p.i., the tumor on each mouse was exposed to an 808 nm laser at 1 W cm^{-2} for 5 min. Another two control groups of mice with and without SPNS-GSH injection were not irradiated. Tumor sizes were measured every 2 days after treatment (**Figure 5**a). All irradiated tumors on mice injected with SPNS-GSH disappeared after laser irradiation, leaving the original tumor site with black scars which fell off in ≈2 weeks after treatment (Figure 5c,d). No tumor re-growth was noted in this treated group over a course of 40 days, after which the study was ended. In marked contrast, tumors in the untreated control group, the irradiation only group (no SPNS-GSH injection), and the SPNS-GSH only group (no laser irradiation) all showed rapid tumor growth, demonstrating that the NIR laser irradiation or SPNS-GSH injection by itself does not affect the tumor development (Figure 5a). Mice in the three control groups showed average life spans of ≈13 days, while mice in the treated group were tumor-free after treatment (SPNS-GSH injection, NIR laser irradiation) and survived over 40 days without a single death (Figure 5b), further demonstrating the excellent efficacy of SPNS-GSH for *in vivo* cancer photothermal therapy.

The potential in vivo toxicity is always a concern for nanomaterial-based biomedicines. To minimize toxicity risks, an ideal nanomaterial-based therapy agent should be effectively cleared out of the body after treatment. The renal excretion has been recognized as a desirable pathway for nanoparticle clearance. Considering their small size, the SPNS-GSH could be potentially cleared out of the body by renal way. The male SD rats were chosen as the animal model in the study. To confirm that the SPNS-GSH can be effectively cleared from body through the

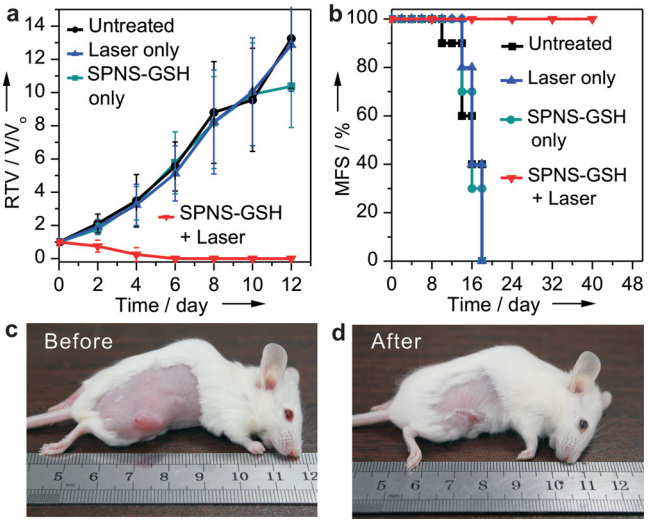

Figure 5. Photothermal ablation of tumors in mice using intravenously injected SPNS-GSH. (a) Relative Tumor Volume (RTV) of different groups after treatment. The tumor volumes were normalized to their initial sizes (n = 10 per group). (b) Mortality Free Survival (MFS) curves of mice bearing 4T1 tumor after various treatments indicated. SPNS-GSH injected mice after photothermal therapy survived over 40 days without any single death. (c,d) Representative photographs of the mice before (c) and after (d) treatment. The laser irradiated tumors on SPNS-GSH injected mice were completely ablated.

NANO MICRO small

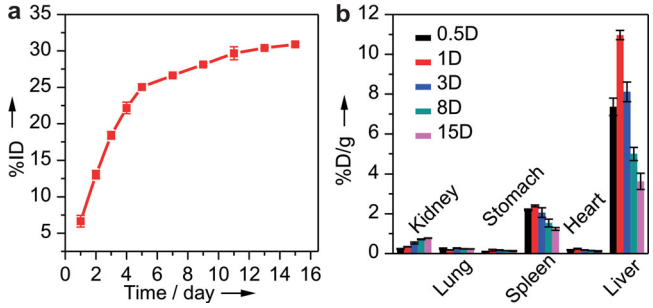

Figure 6. *In vivo* clearance and biodistribution of SPNS-GSH. (a) Urinary cumulative excretion of SPNS-GSH in rats (n = 3) following i.v. administration at a single dose of 10 mg kg^{-1}. The amount of Pd in urinary samples were measured by ICP-MS. (b) Biodistribution of SPNS-GSH in different organs in mice (n = 3) within 15 days after intravenous injection. The percentage of the injected dose was calculated based on the Pd concentration measured by ICP-MS.

renal excretion route into urine, doses of 300 μg of SPNS-GSH were intravenously administered. Urine was collected within a 15-day period after administration. ICP-MS was used to measure the Pd concentration in the urine at different p.i. time points. It was found that more than 6.6% of the SPNS-GSH were excreted out of the body within 1 day p.i. and up to 30.9% after 15 day p.i. (**Figure 6**a). To evaluate the in vivo kinetics, SD rats also were sacrificed at different time points p.i. and major organs were collected to determine the remained Pd by ICP-MS (Figure 6b). As expected, SPNS-GSH mainly accumulated in liver and spleen but could be cleared out from major organs over time. Meanwhile, Pd content in kidney was conversely increased. These observations confirm that SPNS-GSH could be cleared out from body through the renal excretion route into urine.

Moreover, during the study, we did not notice any obvious sign of toxic side effects for SPNS-GSH injected mice at the dose of 400 μg per mouse within 40 days. Neither death nor significant body weight drop was noted in the SPNS-GSH + laser treated group (see Supporting Information, Figure S5). Major organs of SPNS-GSH treated mice whose tumors were eliminated by the photothermal therapy were collected 40 days after the treatment for histology analysis. No noticeable signal of organ damage was observed from haematoxylin and eosin (H&E) stained organ slices (see Supporting Information, Figure S6).

3. Conclusions

In summary, we have demonstrated the facile synthesis of ultra-small Pd nanosheets for efficient in vivo photothermal cancer therapy. The as-prepared ultra-small Pd nanosheets have strong optical absorption in the NIR region and high photothermal conversion efficiency (52.0%) at 808 nm. Surface modification with GSH allows the nanosheets to exhibit prolonged blood circulation and high accumulation in tumors. Upon 808 nm NIR irradiation, the tumors can be completely ablated. More importantly, with the size below the renal filtration limit (<10 nm), the GSHylated Pd nanosheets can be cleared from body through the renal excretion route and into urine. Our work suggests that ultra-small Pd nanosheets have great potential in photothermal cancer therapy.

4. Experimental Section

Synthesis of 4.4 nm Palladium Nanosheets: Pd(II) acetylacetonate ($Pd(acac)_2$, 10.0 mg), poly(vinylpyrrolidone) (PVP, MW = 30 000, 32.0 mg) and NaBr (30.6 mg) were mixed together with N,N-dimethylpropionamide (2 mL) and water (4 mL). After 10 hours on standing, the resulting homogeneous yellow solution was transferred to a glass pressure vessel. The vessel was then charged with CO to 1 bar and heated at 100 °C for 2 h before it was cooled to room temperature. The dark blue products were precipitated by acetone, separated via centrifugation and further purified by an ethanol-acetone mixture.

In Vitro Photothermal Therapy: 0.5 mL solution of purified Pd nanosheets (200 μg mL^{-1}) was mixed with 0.5 mL PEI (5 mg mL^{-1}). The mixture was kept at 4 °C overnight before centrifugation. The particles were then washed with water at least 5 times and then dispersed in 5 mL RPMI 1640 culture medium. Human hepatoma cells (QGY-7703) were cultured in RPMI 1640 medium in 24-well plates with a density of 1×10^5 cells/well. Before incubation with Pd nanosheets, the cells were seeded for 24 h. 0.5 mL of PEI-modified Pd nanosheets in water were added to each well at a concentration of 20 μg mL^{-1}. The incubations were carried out at 37 °C in 5% CO_2 atmosphere for 12 h. After incubation, the cell medium was removed, and the cells were washed before PBS buffer solution was added. After incubation with Pd nanosheets, human hepatoma cells were exposed to a 0.8 W cm^{-2} 808-nm laser for 2 min to induce photothermal cell damage. To identify the cell viability, the dead cells were stained with Trypan Blue.

In Vivo Photothermal Cancer Therapy: 4T1 murine breast cancer cells (from cell storeroom of Chinese Academy of Science) was cultured in RPMI 1640 medium supplemented with 10% FBS and 1% penicillin/streptomycin (all reagents from Hyclone) under 5% CO_2 atmosphere. The 4T1 cells (2×10^6 cells) were harvested, suspended in 50 μL PBS, and subcutaneously injected into the back of female Balb/c mice of each group (n = 10). When the tumors were grown up to a volume of ≈100 mm^3, the mice of each group were intravenously injected with 200 μL of each solution (2 mg mL^{-1} SPNS-GSH solution, PBS) and irradiated with 1 W cm^{-2} continuous NIR laser to tumor region for 5 min after 24-h injection. The tumor size of each group was measured using a skinfold caliper, and tumor volume was calculated using the following equation: tumor volume = $ab^2/2$, where a is the maximum diameter of tumor and b is the minimum diameter of tumor. All studies on animals were done in accordance with the Guidelines for the Care and Use of Laboratory Animals in Fujian.

Supporting Information

Supporting Information is available from the Wiley Online Library or from the author.

Acknowledgements

This work was supported by the MOST of China (2011CB932403, 2014CB932004), the NSFC of China (21131005, 20925103).

[1] M. P. Melancon, M. Zhou, C. Li, *Acc. Chem. Res.* **2011**, *44*, 947–956.
[2] S. Lal, S. E. Clare, N. J. Halas, *Acc. Chem. Res.* **2008**, *41*, 1842–1851.
[3] X. Huang, P. K. Jain, I. H. El-Sayed, M. A. El-Sayed, *Lasers Med. Sci.* **2008**, *23*, 217–228.
[4] P. K. Jain, I. H. El-Sayed, M. A. El-Sayed, *Nano Today* **2007**, *2*, 18–29.
[5] R. Weissleder, *Nat. Biotechnol.* **2001**, *19*, 316–317.
[6] H. Liu, D. Chen, L. Li, T. Liu, L. Tan, X. Wu, F. Tang, *Angew. Chem. Int. Ed.* **2011**, *50*, 891–895.
[7] M. S. Yavuz, Y. Cheng, J. Chen, C. M. Cobley, Q. Zhang, M. Rycenga, J. Xie, C. Kim, K. H. Song, A. G. Schwartz, L. V. Wang, Y. Xia, *Nat. Mater.* **2009**, *8*, 935–939.
[8] X. Huang, I. H. El-Sayed, W. Qian, M. A. El-Sayed, *J. Am. Chem. Soc.* **2006**, *128*, 2115–2120.
[9] S. Tang, X. Huang, N. Zheng, *Chem. Commun.* **2011**, *47*, 3948–3950.
[10] J. T. Robinson, S. M. Tabakman, Y. Liang, H. Wang, H. Sanchez Casalongue, D. Vinh, H. Dai, *J. Am. Chem. Soc.* **2011**, *133*, 6825–6831.
[11] X. Huang, S. Tang, J. Yang, Y. Tan, N. Zheng, *J. Am. Chem. Soc.* **2011**, *133*, 15946–15949.
[12] N. W. S. Kam, M. O'Connell, J. A. Wisdom, H. Dai, *Proc. Natl. Acad. Sci. USA* **2005**, *102*, 11600–11605.
[13] C. M. Hessel, V. P. Pattani, M. Rasch, M. G. Panthani, B. Koo, J. W. Tunnell, B. A. Korgel, *Nano Lett.* **2011**, *11*, 2560–2566.
[14] A. M. Gobin, M. H. Lee, N. J. Halas, W. D. James, R. A. Drezek, J. L. West, *Nano Lett.* **2007**, *7*, 1929–1934.
[15] B. Tian, C. Wang, S. Zhang, L. Feng, Z. Liu, *ACS Nano* **2011**, *5*, 7000–7009.
[16] S. J. Oldenburg, R. D. Averitt, S. L. Westcott, N. J. Halas, *Chem. Phys. Lett.* **1998**, *288*, 243–247.
[17] X. Huang, S. Neretina, M. A. El-Sayed, *Adv. Mater.* **2009**, *21*, 4880–4910.
[18] J. Chen, C. Glaus, R. Laforest, Q. Zhang, M. Yang, M. Gidding, M. J. Welch, Y. Xia, *Small* **2010**, *6*, 811–817.
[19] K. Yang, S. Zhang, G. X. Zhang, X. M. Sun, S. T. Lee, Z. Liu, *Nano Lett.* **2010**, *10*, 3318–3323.
[20] H. K. Moon, S. H. Lee, H. C. Choi, *ACS Nano* **2009**, *3*, 3707–3713.
[21] X. Huang, S. Tang, X. Mu, Y. Dai, G. Chen, Z. Zhou, F. Ruan, Z. Yang, N. Zheng, *Nat. Nanotechnol.* **2011**, *6*, 28–32.
[22] C. Loo, A. Lowery, N. Halas, J. West, R. Drezek, *Nano Lett.* **2005**, *5*, 709–711.
[23] C. Loo, L. Hirsch, M.-H. Lee, E. Chang, J. West, N. Halas, R. Drezek, *Opt. Lett.* **2005**, *30*, 1012–1014.
[24] L. R. Hirsch, R. J. Stafford, J. A. Bankson, S. R. Sershen, B. Rivera, R. E. Price, J. D. Hazle, N. J. Halas, J. L. West, *Proc. Natl. Acad. Sci. USA* **2003**, *100*, 13549–13554.
[25] M. Longmire, P. L. Choyke, H. Kobayashi, *Nanomedicine* **2008**, *3*, 703–717.
[26] B. Nikoobakht, M. A. El-Sayed, *Chem. Mater.* **2003**, *15*, 1957–1962.
[27] M. R. Rasch, K. V. Sokolov, B. A. Korgel, *Langmuir* **2009**, *25*, 11777–11785.
[28] Y. Sun, Y. Xia, *J. Am. Chem. Soc.* **2004**, *126*, 3892–3901.
[29] J. Robinson, K. Welsher, S. Tabakman, S. Sherlock, H. Wang, R. Luong, H. Dai, *Nano Res.* **2010**, *3*, 779–793.
[30] D. K. Roper, W. Ahn, M. Hoepfner, *J. Phys. Chem. C* **2007**, *111*, 3636–3641.
[31] W. H. De Jong, W. I. Hagens, P. Krystek, M. C. Burger, A. J. A. M. Sips, R. E. Geertsma, *Biomaterials* **2008**, *29*, 1912–1919.
[32] M. Semmler-Behnke, W. G. Kreyling, J. Lipka, S. Fertsch, A. Wenk, S. Takenaka, G. Schmid, W. Brandau, *Small* **2008**, *4*, 2108–2111.
[33] C. Zhou, M. Long, Y. P. Qin, X. K. Sun, J. Zheng, *Angew. Chem. Int. Ed.* **2011**, *50*, 3168–3172.
[34] S. H. Kim, Y. M. Choi, M. G. Lee, *J. Pharmacokinet. Biopharm.* **1993**, *21*, 1–17.
[35] M. G. Lee, W. L. Chiou, *J. Pharmacokinet. Biopharm.* **1983**, *11*, 623–640.

Received: November 22, 2013
Published online: April 14, 2014

